Observation of the Spatial Distribution of Gravitationally Bound Quantum States of Ultracold Neutrons and Its Derivation Using the Wigner Function

G. Ichikawa,[1] S. Komamiya,[1] Y. Kamiya,[1] Y. Minami,[1] M. Tani,[1] P. Geltenbort,[2] K. Yamamura,[3] M. Nagano,[3] T. Sanuki,[4] S. Kawasaki,[5] M. Hino,[6] and M. Kitaguchi[7]

[1]*Department of Physics, Graduate School of Science, and International Center for Elementary Particle Physics, The University of Tokyo, 7-3-1 Hongo, Bunkyo-ku, Tokyo 113-0033, Japan*

[2]*Institut Laue-Langevin, BP 156, 6, rue Jules Horowitz, 38042 Grenoble Cedex 9, France*

[3]*Research Center for Ultra-Precision Science and Technology, Graduate School of Engineering, Osaka University, 2-1 Yamadaoka, Suita, Osaka 565-0871, Japan*

[4]*Department of Physics, Graduate School of Science, Tohoku University, 6-3, Aramaki Aza-Aoba, Aoba-ku, Sendai 980-8578, Japan*

[5]*High Energy Accelerator Research Organization, Institute of Particle and Nuclear Studies, 1-1 Oho, Tsukuba, Ibaraki 305-0801, Japan*

[6]*Kyoto University Research Reactor Institute, 2, Asahiro-Nishi, Kumatori-cho, Sennan-gun, Osaka 590-0494, Japan*

[7]*Department of Physics, Graduate School of Science, Nagoya University, Furo-cho, Chikusa-ku, Nagoya 464-8601, Japan*

(Received 8 April 2013; published 19 February 2014)

Ultracold neutrons (UCNs) can be bound by the potential of terrestrial gravity and a reflecting mirror. The wave function of the bound state has characteristic modulations. We carried out an experiment to observe the vertical distribution of the UCNs above such a mirror at the Institut Laue-Langevin in 2011. The observed modulation is in good agreement with that prediction by quantum mechanics using the Wigner function. The spatial resolution of the detector system is estimated to be 0.7 μm. This is the first observation of gravitationally bound states of UCNs with submicron spatial resolution.

DOI: 10.1103/PhysRevLett.112.071101 PACS numbers: 04.80.-y, 03.65.Ta

Terrestrial gravity is the most common force experienced in everyday life. However, experimental measurements of quantum-mechanical bound states in Earth's gravitational field were started only in the past decade by the pioneering works of Nesvizhevsky *et al.* using ultracold neutrons (UCNs) [1,2]. UCNs are neutrons with kinetic energies lower than the Fermi pseudopotential of materials (e.g., Ni, with ~200 neV) and are, hence, totally reflected by the material surfaces at any angle of incidence. The wave function $\psi(z)$ of an UCN in the terrestrial gravitational field obeys the Schrödinger equation in the vertical direction z. The eigenstates of this system are linear combinations of Airy functions [3]. The vertical probability distribution of UCN bound states, namely, the sum of the absolute squares of eigenfunctions, has a characteristic modulation. The eigenstate is specified by two scales, the length $[\hbar^2/(2m^2g)]^{1/3} = 5.87$ μm and the energy $(mg^2\hbar^2/2)^{1/3} = 0.602$ peV, where $\hbar$ is the reduced Planck constant, m is the neutron mass, and g is the gravitational acceleration. There are, therefore, two ways to observe the bound state, measuring its energy or its position. Recently, first measurements of the differences between eigenenergies using the transitions of UCNs between quantum states in the terrestrial gravitational potential have been reported [4]. The ability of experiments to observe the spatial distribution of the bound state is limited by the spatial resolution (about 2 μm) of current slow neutron detectors.

To observe the spatial distribution of gravitationally bound states with high precision, we developed a novel technique, shown in Fig. 1, with three main components [5]. The Cartesian coordinate system (x, y, z) is defined in Fig. 1(b). Incident UCNs pass through the collimating guide in which they settle into gravitationally bound states above the flat bottom mirror. The ceiling removes UCNs whose wave functions significantly penetrate the ceiling. The height distribution of the surviving UCNs is magnified by a cylindrical rod which acts as a convex mirror. After reflection at the rod surface, UCNs are detected by a CCD-based pixelated detector. Z is the axis on the pixelated detector corresponding to the magnified height z. The collimating guide and magnification rod have a width of 50 mm along y. Using this setup, we performed an experiment to observe the spatial distribution of gravitationally bound states during a period of 17 days in August 2011 at the Institut Laue-Langevin (ILL).

We used the UCN beam line PF2 [6] at ILL, the world's highest intensity steady UCN source. The horizontal velocity (v_x) distribution of UCNs was measured using the standard time-of-flight technique. The measured velocity distribution is nearly Gaussian, with a mean of 9.4 m/s and standard deviation of 2.8 m/s.

The energy of UCNs is quantized inside the collimating guide made of glass, with a height $h = 100$ μm. The ceiling of the guide removes UCNs with high vertical energy due to its microscopic surface roughness, with an arithmetic mean of 0.4 μm. Once such a neutron is reflected by the ceiling, the large horizontal velocity component is converted into a vertical velocity component. The chance to hit

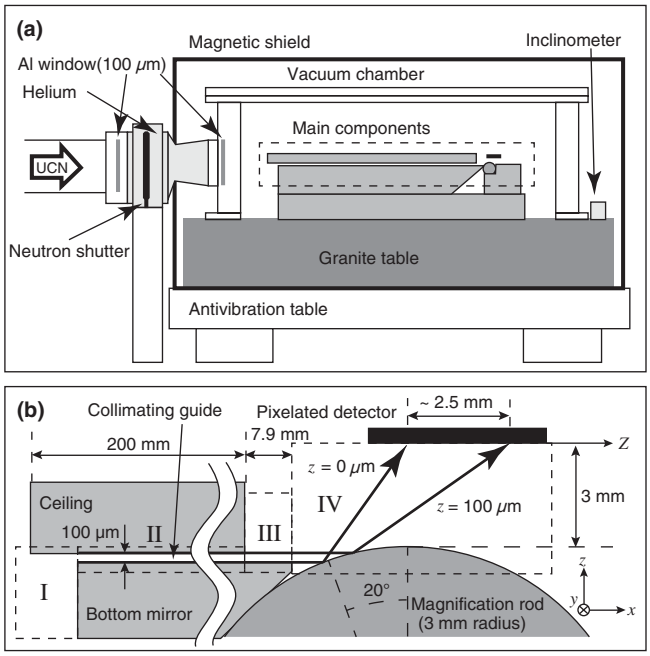

FIG. 1. Experimental setup. (a) General view and (b) the main components. The two thick bent arrows in (b) correspond to the trajectories of neutrons flying horizontally above the bottom mirror with the height of the bottom mirror $z = 0$ μm and that of the ceiling $z = 100$ μm. The 45° slope of the bottom mirror and the rod are designed to come in contact with each other. The roman numerals denote the calculation steps.

the ceiling again is then enormously enhanced. Numerous collisions cause UCN loss by absorption or upscattering. In addition, an absorptive Gd-Ti-Zr alloy (54/35/11) was deposited on the glass by vacuum evaporation [7] at the Kyoto University Research Reactor Institute. The thickness of the layer is 200 nm, and its potential is calculated to be $-13.9 - 26.5i$ neV.

At the end of the collimating guide, a cylindrical glass rod of radius 3 mm magnifies the distribution of UCN like a convex mirror. The geometrical arrangement of the magnification system is shown in Fig. 1(b). The distribution of 100 μm in height z is magnified to ~2.5 mm in the position Z on the detector; hence, the average magnification power is about 25. The glancing angle was only 20° in order to make the critical energy of reflection high. Differences in v_x cause dispersion of the parabolic trajectories and smear the distribution. This dispersion is estimated to be less than 0.1 μm of the height z. The rod was precisely ground by Crystal Optics, Inc., and finely polished at the Research Center for Ultra-Precision Science and Technology, Osaka University. Furthermore, a Ni layer of 200 nm was deposited on the polished glass surface, increasing the potential from 100 to 200 neV so that all UCNs exiting the guide were totally reflected. The Ni deposited surface has an arithmetic mean roughness of 1.9 nm, much smaller than the wavelength of UCN ~100 nm. Hence, the diffused reflection from the surface roughness of the rod can be neglected.

For high resolution two-dimensional detection, a CCD was used. Since slow neutrons would pass through the sensitive volume of CCDs without ionization, they must first be converted to charged particles. To retain the intrinsic spatial resolution, a 200 nm thin ^{10}B neutron converter was evaporated directly onto a CCD. After neutron capture, α and ^{7}Li particles are released. A back-thinned CCD [8] was the base of the detector, with a pixel size is 24 μm × 24 μm and sensitive area of 24.576 mm × 6.000 mm. The length along the Z axis is 6 mm. An incident charged particle creates electron-hole pairs inside the Si layer and loses energy. About 300 000 electrons per MeV are created and spread before reaching electrodes and being detected as a two-dimensional cluster. The barycenter of the deposited charges corresponds to the incident position of the charged particle. The spatial resolution along the Z axis was measured to be 3.35 ± 0.09 μm [9].

The setup was installed inside a vacuum chamber to prevent neutrons from interacting with air. We evacuated the chamber to 10 Pa before the experimental run. The vacuum pump was disconnected during the measurement to reduce vibration.

A neutron shutter with Cd blades was installed inside an acrylic box as shown in Fig. 1(a) to shut off the UCN beam during the readout of the CCD. The box was connected to the beam pipe and the vacuum chamber by plastic bellows, to prevent the transmission of vibrations. The shutter box and the plastic bellows were filled with helium gas to minimize scattering.

The magnetic shield of mu-metal covering the experimental apparatus reduces the external magnetic field by about 1/100. As shown in Fig. 1(a), the detector system was installed on granite and antivibration tables [10] to reduce vibration from the floor.

The horizontality of the detector system was better than 0.1 mrad and monitored by an inclinometer. The remaining effects due to external magnetic field, vibration, and horizontality were estimated to be negligible.

The distribution of UCNs on the pixelated detector can be calculated using quantum mechanics. The state of an UCN can, in general, be written as a superposition of the nth energy eigenstates as $\Psi(z,t) = \sum_n a_n \psi_n(z) \exp(-iE_n t/\hbar)$, where a_n satisfies $\sum_n |a_n|^2 = 1$ and $\psi_n(z)$ is normalized to give $\int dz |\psi_n(z)|^2 = 1$. The experimental result is an average over many incoherent UCNs. Since the phase of a_n is randomly and uniformly distributed, the average of the absolute squared value of the superposition becomes $|\Psi(z)|^2 = \sum_n |a_n|^2 |\psi_n(z)|^2$, where the time dependence and interference terms are averaged out. In general, the quantum state of UCNs is treated as a mixed state. The state is described as a density matrix, $\hat{\rho} = \sum_n p_n |\psi_n\rangle\langle\psi_n|$, where $p_n = |a_n|^2$ is the probability of the nth state and $|\psi_n\rangle$ is the corresponding state vector. The calculation was performed in four steps (I, II, III, IV) from upstream towards the detector, as shown in Fig. 1(b). In the first three steps, the

probability of the eigenstate p_n at the end of the guide is calculated and then, in the last step, the UCN distribution on the pixelated detector is derived. Each step is discussed in the following paragraphs.

(I) The probabilities of the eigenstates just after the entrance of the collimating guide are assumed to be uniform. It should be noted that the eigenstates with vertical energy larger than mgh ($h = 100$ μm) inside the guide are different from the case without the ceiling, because the wave function becomes zero at the height of the ceiling. In the following, values with tildes denote the case with the ceiling at $z = h$.

(II) For UCN loss inside the guide, we assume a phenomenological loss rate of the nth state as $\Gamma_n + B_n$, where Γ_n and B_n are, respectively, the loss by the ceiling and the bottom mirror. Γ_n is assumed to be proportional to the probability of finding an UCN in the roughness region as $\Gamma_n = \gamma \int_{h-2\delta}^{h} dz|\tilde{\psi}_n(z)|^2$, where γ is the constant for the loss and $\delta = 0.4$ μm is the arithmetic mean roughness of the ceiling (2δ is the average width of the roughness region) [11]. B_n is assumed to be proportional to the bouncing number per unit time of a bouncing motion above a floor in classical mechanics, $B_n = \beta(g/2\sqrt{2})\sqrt{m/\tilde{E}_n}$, where β is the constant for the loss. Hence, the probability at the guide exit $\tilde{p}_n$ is written in terms of that at the guide entrance $\tilde{p}_n(0)$ as $\tilde{p}_n \propto \tilde{p}_n(0)\langle \exp[-l/v_x(\Gamma_n + \mathrm{B}_n)]\rangle_{v_x}$, where l is the length of the guide, $\langle\rangle_{v_x}$ indicates the average over the measured distribution of v_x, and the normalization constant is chosen to satisfy $\sum_n \tilde{p}_n = 1$.

(III) At the exit of the guide, the wave function changes because the ceiling suddenly disappears. From the sudden approximation, the wave function is continuous at the time of the sudden change as $\sum_m \tilde{a}_m \tilde{\psi}_m = \sum_n a_n \psi_n$, where the left- (right-)hand side corresponds to the wave function with (without) the ceiling. Using the properties of a complete orthonormal system, we obtain $p_n = \sum_m \tilde{p}_m |\int_0^h dz \psi_n(z)\tilde{\psi}_m(z)|^2$, where the probabilities satisfy $p_n = |a_n|^2$ and $\tilde{p}_m = |\tilde{a}_m|^2$. In this equation, the cross terms are canceled due to random phases. The resulting probabilities of the eigenstates p_n are shown in Fig. 2(a). The suppression of small n eigenstates has been reported by past experiments [2,11].

(IV) The detected position on the detector after magnification depends not only on the height z but also on the vertical velocity v_z at the end of the guide. Hence, we use a kind of probability density in phase space given by the Wigner function [12]. The Wigner function is defined as

$$W(z, p_z) = \frac{1}{2\pi\hbar}\int_{-\infty}^{\infty} d\xi \psi^*\left(z - \frac{1}{2}\xi\right)\psi\left(z + \frac{1}{2}\xi\right) \times \exp\left(-\frac{ip_z\xi}{\hbar}\right),$$

where z is the height, p_z is the momentum along z, and ψ is the wave function. The Wigner function in z-v_z phase space

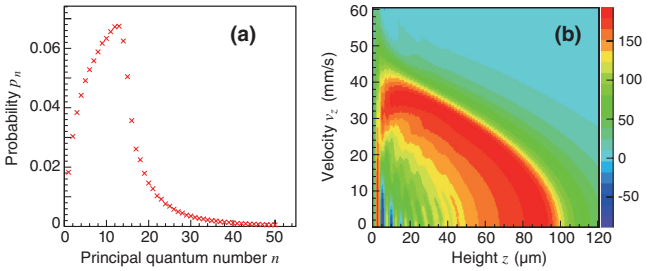

FIG. 2. (color) The resulting probabilities for eigenstates p_n (a) and the corresponding Wigner function $W(z, v_z)$, the sum of the Wigner functions $n \leq 50$ with the weights of the probabilities for the eigenstates (b). $W(z, v_z)$ for $v_z > 0$ is shown here because $W(z, v_z) = W(z, -v_z)$. The color scale in (b) is in arbitrary units. The best-fit parameters are used in both panels.

can be obtained by replacing p_z with mv_z. The Wigner function has properties of $\int_{-\infty}^{\infty} dp_z W(z, p_z) = |\psi(z)|^2$ and $\int_{-\infty}^{\infty} dz W(z, p_z) = |\varphi(p_z)|^2$, where $\varphi(p_z)$ is the momentum space wave function. The Wigner function of a mixed state $\hat{\rho} = \sum_n p_n |\psi_n\rangle\langle\psi_n|$ is a simple sum $W(z, p_z) = \sum_n p_n W_n(z, p_z)$, where W_n is the Wigner function for the nth eigenstate. The Wigner function obtained for this system is shown in Fig. 2(b). We calculate the correspondence of the phase space point at the guide end and the detection point on the detector by the classical trajectory. This treatment is supported by the fact that, if the potential of the system has terms only up to the second order in the position, the motion of the Wigner function in the phase space can be obtained by the equation of motion in classical mechanics [13]. In this case, the potential has only a first-order term of mgz. The whole phase space was divided into a mesh with a size of $\Delta z \times \Delta v_z = 0.1$ μm $\times$ 0.1 mm/s and each mesh point was weighted by the Wigner function $W(z, v_z)$.

The predicted distribution was fitted to the data using a binned maximum-likelihood method. Six parameters were used in the fit: θ, Z_0, d, γ, β, and s. θ denotes the rotation of the pixelated detector in the detector plane. The position of the data Z is rotated by θ to be $Z \to Z'$. Z_0 is the offset for the position of predicted events Z_{pred}. The relation of the coordinates is $Z' = Z_{\mathrm{pred}} + Z_0$. d is the difference between the actual and design heights of the pixelated detector; hence, d effectively modifies the magnification power. $d > 0$ denotes that the actual position is higher than the design, corresponding to a higher magnification. γ and β are the parameters describing losses inside the guide. s is the ratio of the signal to the total events. A flat background in Z is assumed. The predicted distribution is normalized to have the same sum of weights as number of events in the data.

The classical mechanical prediction was also fitted to the data. The probability distribution in phase space just after the entrance of the guide is assumed to be uniform. The same parameter definitions of θ, Z_0, d, and s were used, while, for UCN loss inside the guide, two parameters, c and

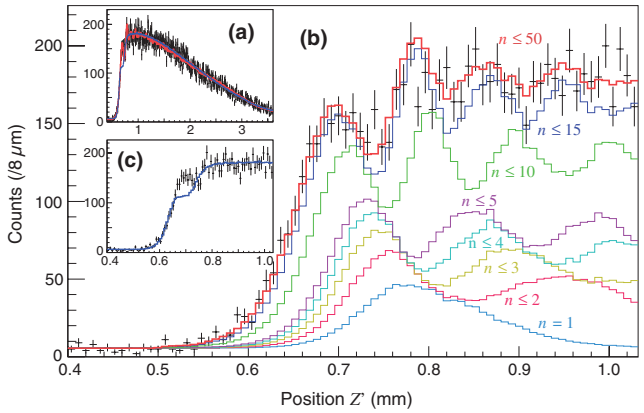

FIG. 3. (color) (a) Observed and fitted distributions of UCNs at the pixelated detector for the whole region. Points with errors show that for the data, and the red (blue) line corresponds to the quantum-mechanical (classical) prediction with the best-fit parameters. (b) Cumulations of the eigenstates of the quantum-mechanical prediction in the lower Z' region. (c) Distributions of the classical mechanical prediction and the data in the lower Z' region.

b, were used instead of γ and β. In this case, when an UCN hits the ceiling (floor), it is removed with a probability of c (b) and specularly reflected with a probability of $1-c$ ($1-b$).

Events within the whole expected region $0.4 \leq Z' \leq 3.6$ mm are selected and used to fill a histogram with 400 bins of width 8 μm. Eigenstates with $n \leq 50$ are used in the calculation. The best-fit parameters for quantum (classical) mechanics are $s = 0.95 \pm 0.02 (0.94^{+0.01}_{-0.02})$, $Z_0 = -1.009^{+0.001}_{-0.002} (-0.970^{+0.002}_{-0.007})$ mm, $d = -0.015^{+0.004}_{-0.006}$ $(-0.23^{+0.03}_{-0.02})$ mm, $\theta = -1.254 \pm 0.001$(fixed to -1.254) deg, $\gamma = (9.5^{+0.7}_{-0.9}) \times 10^4$ s^{-1} ($c = 0.01 \pm 0.01$), and $\beta = 0.38^{+0.04}_{-0.03}$ ($b = 0.40 \pm 0.02$). The χ^2 per degrees of freedom (NDF) is $\chi^2/\mathrm{NDF} = 377.6/394 (439.2/395)$ and the corresponding p value is 0.715 (0.062). The distributions of the data and the predictions of the best fits are shown in Fig. 3. The form of the several modulations observed in the data is in good agreement with the best-fit prediction using quantum mechanics [Fig. 3(b)]. The modulation of the quantum-mechanical prediction is mostly due to eigenstates with $n \leq 15$. This result favors the quantum-mechanical prediction. In the classical mechanical prediction [Fig. 3(c)], the two rising edges at $Z' \sim 0.65$ mm and $Z' \sim 0.75$ mm of the distribution are due to downward- and upward-going neutrons just before reflection by the rod.

The estimated systematic uncertainties are summarized in Table I. ΔZ is the uncertainty in Z and Δz that in z. These uncertainties are calculated for neutrons with $z = 0$ and $v_z = 0$, where the magnification power is the minimum value 16.5. The total uncertainty of z is $\Delta z = 0.7$ μm. No detector effect was found which could fake the observed modulation. The predicted modulation is also robust against variations of fit parameters within their uncertainties.

TABLE I. Measured systematic uncertainties (with 1σ).

Source	ΔZ	Δz
v_x dispersion	1.2 μm	0.1 μm
Aberration of rod	4.8 μm	0.3 μm
Spatial resolution of detector	3.4 μm	0.2 μm
Roughness of detector surface	10.6 μm	0.6 μm
Total	12.1 μm	0.7 μm

In conclusion, we observed the spatial distribution of gravitationally bound states of UCNs using a novel technique. The vertical distribution of UCNs was magnified by a cylindrical rod and detected by a pixelated detector. The measured UCN distribution on the pixelated detector can be derived using the Wigner function. The shape of several peaks of the modulation of the UCN distribution in the lower Z' region is in good agreement with the quantum-mechanical prediction. This is the first observation of gravitationally bound states with submicron resolution.

We would like to thank H. Shimizu of Nagoya University, V. V. Nesvizhevsky of Institut Laue-Langevin, and H. Abele of the Vienna University of Technology for their advice regarding the experiment. We appreciate M. Ueda of the University of Tokyo for the corroboration on the usage of the Wigner function. We are grateful to T. Brenner of Institut Laue-Langevin for his support during and before the experiment and to S. Sonoda of Kyoto University for his early work on the pixelated detector. We also thank O. Kirino of Crystal Optics, Inc., for his work on polishing the cylindrical rod, H. Takeuchi of Panasonic Co., Ltd., for measuring the aberration of the rod, and D. Jeans of the University of Tokyo for proofreading the manuscript. This work was supported by JSPS KAKENHI Grants No. 20340050 and No. 24340045 and Grant-in-Aid for JSPS Fellows No. 22.1661.

[1] V. V. Nesvizhevsky *et al.*, Nature (London) **415**, 297 (2002).
[2] V. V. Nesvizhevsky *et al.*, Eur. Phys. J. C **40**, 479 (2005).
[3] L. D. Landau and E. M. Lifshitz, *Quantum Mechanics: Non-Relativistic Theory* (Butterworth-Heinemann, Oxford, England, 1981), 3rd ed., p. 74; J. J. Sakurai and J. J. Napolitano, *Modern Quantum Mechanics* (Addison-Wesley, San Francisco, 2010), 2nd ed., p. 108.
[4] T. Jenke, P. Geltenbort, H. Lemmel, and H. Abele, Nat. Phys. **7**, 468 (2011).
[5] T. Sanuki, S. Komamiya, S. Kawasaki, and S. Sonoda, Nucl. Instrum. Methods Phys. Res., Sect. A **600**, 657 (2009).
[6] A. Steyerl *et al.*, Phys. Lett. A **116**, 347 (1986).

[7] S. Tasaki, T. Ebisawa, T. Akiyoshi, T. Kawai, and S. Okamoto, Nucl. Instrum. Methods Phys. Res., Sect. A **355**, 501 (1995).
[8] Hamamatsu Photonics K.K., S7030-1008.
[9] S. Kawasaki, G. Ichikawa, M. Hino, Y. Kamiya, M. Kitaguchi, S. Komamiya, T. Sanuki, and S. Sonoda, Nucl. Instrum. Methods Phys. Res., Sect. A **615**, 42 (2010).
[10] Herz Co., Ltd., AVI-350MLP.
[11] A. Westphal, H. Abele, S. Baeßler, V. V. Nesvizhevsky, K. V. Protasov, and A. Y. Voronin, Eur. Phys. J. C **51**, 367 (2007).
[12] E. P. Wigner, Phys. Rev. **40**, 749 (1932); M. Hillery, R. F. O'Connel, M. O. Scully, and E. P. Wigner, Phys. Rep. **106**, 121 (1984).
[13] W. P. Schleich, *Quantum Optics in Phase Space* (Wiley-VCH, Berlin, 2001), p. 76.